Journal of Power Sources 196 (2011) 6228–6231

Contents lists available at ScienceDirect

Journal of Power Sources

journal homepage: www.elsevier.com/locate/jpowsour

Short communication

# Platinum–antimony doped tin oxide nanoparticles supported on carbon black as anode catalysts for direct methanol fuel cells

Chengqiang Pan, Yingzhi Li, Yuehui Ma, Xin Zhao, Qinghua Zhang*

*State Key Laboratory for Modification of Chemical Fibers and Polymer Materials, College of Materials Science and Engineering, Donghua University, Shanghai 201620, PR China*

ARTICLE INFO

*Article history:*
Received 10 March 2011
Accepted 12 March 2011
Available online 12 April 2011

*Keywords:*
Platinum
Antimony tin oxide
Anode catalyst
Direct methanol fuel cell

ABSTRACT

Antimony doped tin oxide supported on carbon black (ATO/C) has been synthesized using an *in situ* co-precipitation method, and platinum–ATO/C nanoparticles have been prepared using a consecutive polyol process to enhance the catalyst activity for the methanol oxidation reaction. The Pt–ATO/C electrocatalyst is characterized by X-ray diffraction (XRD), transmission electron microscopy (TEM), scanning electron microcopy (SEM), energy dispersive X-ray spectroscopy (EDS) and cyclic voltammetry. The Pt–ATO/C catalyst exhibits a relatively high activity for the methanol oxidation reaction compared to Pt–$SnO_2$/C or commercial Pt/C catalyst. This activity can be attributed to the high electrical conductivities of the Sb-doped $SnO_2$, which induces the electronic effects with Pt catalysts. Pt–ATO/C is a promising methanol oxidation catalyst with high activity for the reaction in direct methanol fuel cells.



## 1. Introduction

Direct methanol fuel cells (DMFCs) are promising portable power sources due to their suitable power range for small electronic devices, high energy efficiency, and ambient operating conditions [1–7]. However, the commercialization of DMFCs for portable-power-source markets is still a challenge. One of the important hurdles is the development of a new structural and compositional anode catalyst with a high activity in the methanol oxidation reaction (MOR).

To overcome this problem, much effort has gone into attempting to develop a sufficiently selective and active electrocatalyst for the DMFC anode. One approach is to use Pt enhanced with ceramic oxides, such as $TiO_2$ [8–10], $V_2O_5$ [11,12], $ZrO_2$ [13,14] and $SnO_2$ [15,16], to increase the CO tolerance and thus favorably affect the MOR. However, these semiconducting oxides cannot effectively exhibit high catalyst effectiveness when their surface is coated with Pt due to their low electrical conductivity and relatively low specific surface area. Therefore, it remains important to the catalytic activity and use of the catalyst to find an ideal support for nanostructural Pt. A highly efficient catalyst support is necessary to ensure high electrical conductivity and a relatively high specific surface area on which Pt can be uniformly dispersed.

Metal-doped tin oxides are typical n-type semiconducting materials with good stability and high electrical conductivity [17–20]. They enable the adsorption of OH species at low potentials, promoting the electro-oxidation of CO and low-molecular-weight alcohols, such as methanol and ethanol [21,22]. In previous reports [15,16], Pt–$SnO_2$/C catalysts were synthesized and exhibited good electrocatalytic activity; however, the electrocatalytic activity and electron conduction of these catalysts are limited by the relatively inferior electrical conductivity of $SnO_2$.

In this report, Pt nanoparticles containing adjacent ATO supported on carbon black were prepared by a consecutive polyol process with the goal of achieving high activity for the MOR. ATO with good electrical conductivity and high specific surface area exhibited good dispersion on the carbon black carrier. The obtained catalysts with 20 wt.% Pt loading on the ATO/C support have excellent electrocatalytic activity and CO tolerance for the direct electro-oxidation of methanol.

## 2. Experimental

### 2.1. Synthesis of Pt–ATO/C nanoparticles

ATO/C composites were synthesized *in situ* by co-precipitation. The following were added to 300 ml of anhydrous alcohol with stirring: 1.754 g of $SnCl_4{\cdot}5H_2O$, 0.057 g of $SbCl_3$ and 3.176 g of carbon black. An aqueous solution of $NH_3{\cdot}H_2O$ was dripped into the above solution until the pH reached 9. After 2 h, the solution was washed with anhydrous alcohol, centrifuged and dried at 100 °C for 2 h. The obtained dark-yellow solid was heated in a muffle furnace at 600 °C for 2 h in ambient air. The ATO content in the prepared composites was 20 wt.%. For comparison, $SnO_2$/C composites were also obtained using the same process.

* Corresponding author. Tel.: +86 21 67792854; fax: +86 21 67792854.
*E-mail address:* qhzhang@dhu.edu.cn (Q. Zhang).

0378-7753/$ – see front matter © 2011 Elsevier B.V. All rights reserved.
doi:10.1016/j.jpowsour.2011.03.027

The polyol method was used to prepare Pt–ATO/C nanoparticles [7]. $H_2PtCl_6 \cdot xH_2O$ (400 mg) was dissolved in 100 ml of ethylene glycol. The solution was refluxed in a three-necked flask at 140 °C for 30 min in the nitrogen atmosphere. Adequate amounts of the resultant Pt colloid were mixed with an aqueous solution of the ATO/C nanoparticles. After stirring for 2 h, 2 M $H_2SO_4$ was added to adjust the pH to 4, and the solution was filtered and dried. The obtained electrocatalysts were heated in an oven at 160 °C in the ambient air to eliminate the remaining organic materials. The nominal Pt content in the prepared electrocatalysts was 20 wt.%. A parallel sample of the Pt–$SnO_2$/C catalyst with the same Pt content was prepared using the above method.

### 2.2. Measurement

The morphology of Pt–ATO/C composites was observed on a high-resolution transmission electron microscopy (HRTEM, JEOL model JEM-2100) at a voltage of 200 kV. The surface morphology of the powder was observed by a scanning electron microscope (SEM) (JEOL JSM-5600LV). The XRD patterns of the samples were obtained by a Bruker powder-diffraction system (model D8 Advanced) using Cu $K_\alpha$ as the radiation source at an operating voltage of 40 kV.

Cyclic voltammograms were measured in a conventional three-electrode electrochemical cell using a glassy-carbon electrode as the working electrode, platinum wire as the counter electrode, and a saturated calomel electrode (SCE) as the reference electrode, according to a previous report [21]. The glassy-carbon electrode was polished with 1 μm, 0.3 μm, and 0.05 μm $Al_2O_3$ slurries and washed ultrasonically with de-ionized water before use. For the three electrocatalysts of Pt–ATO/C, Pt–$SnO_2$/C and Pt/C, inks were prepared by mixing one of the electrocatalysts, de-ionized water, 2-propanol, and 5 wt.% Nafion solution as a binding material. The inks were dropped onto glassy carbon (GC) electrodes, and the electrodes were dried in a vacuum oven. Electrochemical experiments were performed on a CHI 660C instrument. The solution of 1.0 M $H_2SO_4$/1.0 M $CH_3OH$ was purged with nitrogen gas before the measurements. To identify the activities of the electrocatalysts, voltammetry was conducted in the potential between −0.2 and 1.0 V versus SCE at a scan rate of 50 mV $s^{-1}$. Chronoamperometry was performed in 1.0 M $H_2SO_4$/1 M $CH_3OH$ for 1 h. The resistivity of ATO powders was tested on Keithley 6517A source measure unit.

## 3. Results and discussion

### 3.1. XRD analysis

Fig. 1 shows the XRD patterns of the Pt–ATO/C, Pt–$SnO_2$/C, ATO/C and $SnO_2$/C samples. As shown in curve (a) in the figure, the diffraction peaks around 40°, 47°, 68° and 81° are accordance with the Pt (1 1 1), (2 0 0), (2 2 0) and (3 1 1) planes of the face-centered cubic structure of Pt (JCPDS No. 87-0640), respectively [23]. Comparing the XRD patterns of (a)–(d), the high diffraction peaks of (1 1 0), (1 0 1) and (2 1 1) planes are clearly observed and agree well with the reflections of the tetragonal rutile structure of pure $SnO_2$ (d) (JCPDS No. 88-2348). Compared to $SnO_2$/C, the diffraction peaks (1 1 0), (1 0 1), (2 0 0) and (2 1 1) of ATO/C are broader, and no $Sb_2O_3$ or $Sb_2O_5$ appears in the XRD patterns. The results indicate that all antimony ions completely incorporate into the lattice of bulk $SnO_2$ and that the tin ions are replaced with the two ionic states of $Sb^{3+}$ and $Sb^{5+}$. Therefore, no diffraction peak of $Sb_2O_3$ or $Sb_2O_5$ is found. This result is in accordance with previous reports [24,25]. $Sb^{3+}$ has a larger ionic radius (0.76 Å) and $Sb^{5+}$ has a smaller ionic radius (0.60 Å) than the Sn ionic radius (0.69 Å) [26]. Most $Sb^{3+}$ transfer into $Sb^{5+}$ at higher calcination temperatures, and the incorporation of $Sb^{5+}$ changes the lattice parameter and induces a defect into the $SnO_2$ lattice, which is why ATO/C diffraction peaks are broader than those of $SnO_2$/C.

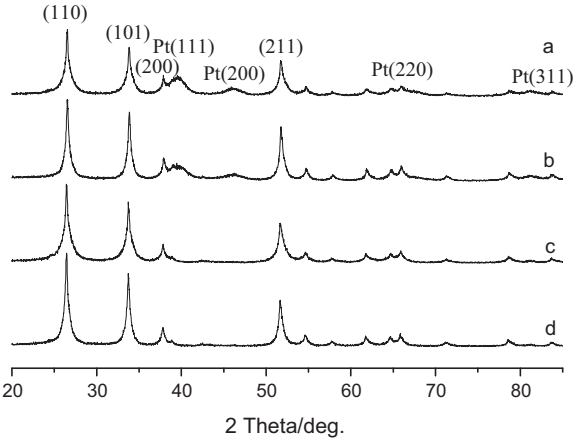


**Fig. 1.** XRD patterns of (a) Pt–ATO/C, (b) Pt–$SnO_2$/C, (c) ATO/C, and (d) $SnO_2$/C.

The crystalline size can be calculated by Scherrer's equation $D_{(h\,k\,l)} = k\lambda/\beta \cos\theta$, where $D_{(h\,k\,l)}$ is a correlation length or an individual crystallite size (nm), ($h\,k\,l$) are the Miller indices of the planes perpendicular to the direction related to the crystal size, $\lambda$ = 0.154 nm is the mean wavelength of the copper radiation source, $\beta$ is the full-width half-maximum (FWHM) of the Bragg peak observed at the Bragg angle $\theta$ (in radian), and $K$ is a constant depending on the diffraction technique (here $K$ = 0.89). The average crystal size of the $SnO_2$ (1 1 0), (1 0 1) and (2 1 1) lattice planes is 16.0 nm. The value for the Pt (1 1 1) and Pt (2 1 1) plane of Pt–ATO/C is 8.6 nm, and the value for Pt–$SnO_2$/C is 8.4 nm. The positions of the Pt diffraction peaks are constant in the Pt–$SnO_2$/C catalysts, indicating that the material is composed of Pt without an alloy phase. This result is further confirmed by EDX analysis of Pt particles in next section.

### 3.2. Morphology

Fig. 2 shows the TEM images of the Pt–ATO/C particles with different magnifications, and the semitransparent region is the carbon-black support. The Pt–ATO nanoparticles appear to be uniformly distributed over the carbon support, but some agglomeration appears in some areas. In image (b), the black spheres are Pt nanoparticles with an average diameter of 8 nm and the grey spheres are ATO particles with an average diameter of 15 nm, which are similar to the XRD results.

The high-resolution images (c) and (d) show that the grey crystal lattice with 3.36 Å is the $SnO_2$ (1 1 0) lattice plane and that the black crystal lattice with 2.27 Å is the Pt (1 1 1) lattice plane. Therefore, this result further confirms that ATO and Pt crystals are involved in these particles.

Fig. 3 shows the FESEM image of the Pt–ATO/C particles. The ATO is uniformly distributed on the carbon-black support in the bright region, although a slight agglomeration appears elsewhere. The signals of C, Sb, Sn, O and Pt can be easily detected by EDX at different sites, as shown in the EDX image. These results further confirm the successful preparation of the Pt–ATO/C composite.

### 3.3. Electrochemical properties of Pt–ATO/C composites

The $n$(Sb):$n$(Sn) molar ratio plays an important role in ATO resistivity and specific surface area. As shown in Fig. 4, the resistivity of ATO particle reaches a minimum of 2.29 Ω cm at the molar ratio $n$(Sb) to $n$(Sn) being 5 at.%. In other word, ATO with 4 wt.% Sb dopant exhibits a relatively high conductivity. As mentioned in Section 2,

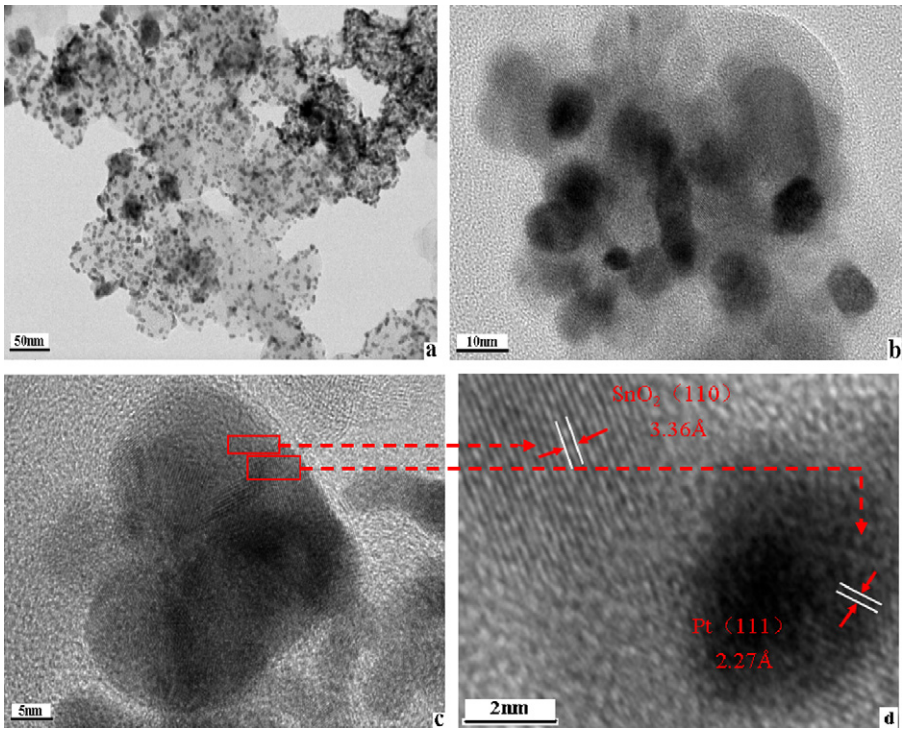


**Fig. 2.** TEM images of Pt–ATO/C at different magnifications.

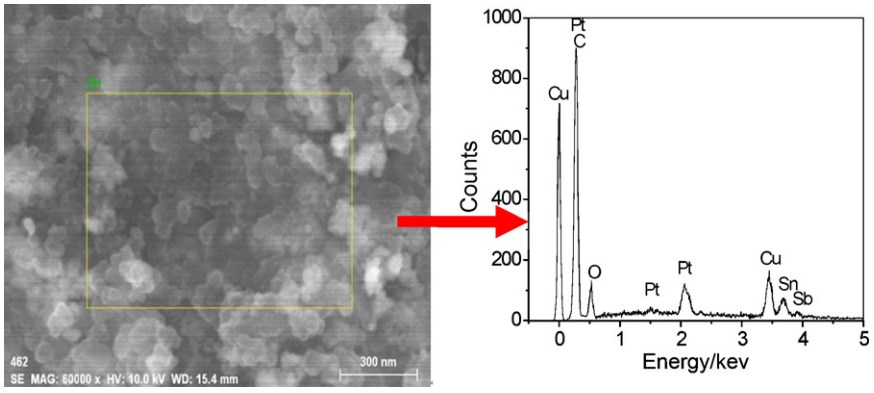


**Fig. 3.** FESEM and EDX images of Pt–ATO/C composites.

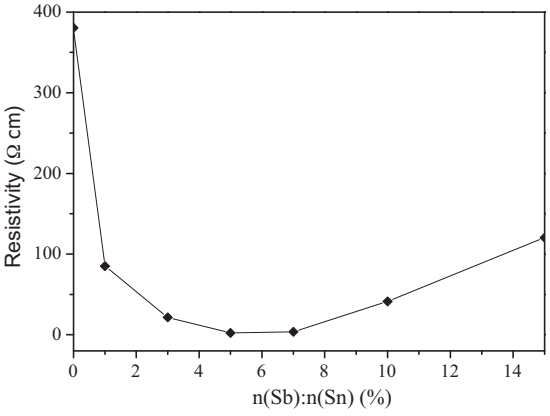


**Fig. 4.** Dependence of resistivity of ATO on Sb dopant.

the ATO content in the Pt–ATO/C is 20 wt.%, such that the Sb content is 0.8 wt.% in the Pt–ATO/C.

The Pt–ATO/C samples are tested for their catalytic activity in the electro-oxidation of methanol. To investigate the role of the ATO in the catalyst, a parallel sample of Pt–$SnO_2$/C was prepared with the same Pt content as Pt–ATO/C, and a commercial E-TEK Pt/C catalyst with same Pt content of 20% was used for comparison. Fig. 5 shows the voltammetric curves for the synthesized and reference catalysts in 1 M $CH_3OH$ and 1 M $H_2SO_4$ as the supporting electrolyte. The peak currents due to methanol oxidation in the forward scan for Pt–ATO/C, Pt–$SnO_2$/C and the E-TEK Pt/C catalyst are 8.9, 5.9 and 3.5 mA $cm^{-2}$, respectively. Pt–ATO/C exhibits a current density that is 2.5-fold greater compared to the Pt/C catalyst and 1.5-fold greater compared to the Pt–$SnO_2$/C catalyst. It is clearly found that Pt–ATO/C promotes the electro-oxidation of COads much more than the Pt–$SnO_2$/C catalyst does due to the larger number of oxygen vacancies generated in the doped $SnO_2$ by antimony. Therefore, Pt–ATO/C shows significant activity for methanol oxidation. Furthermore, the onset potential of Pt–ATO/C is lower than that of Pt–$SnO_2$/C or Pt/C, indicating that the Pt–ATO/C

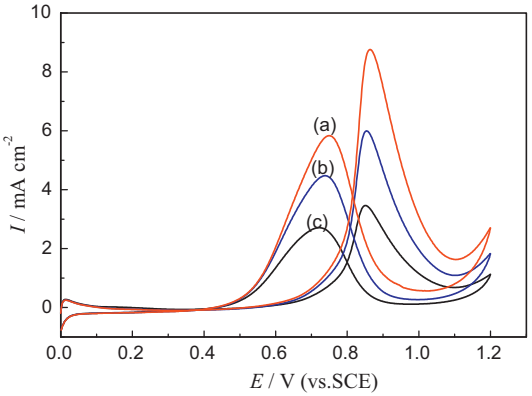


**Fig. 5.** Cyclic voltammograms (CVs) of various electrodes at 50 mV $s^{-1}$ in 1.0 M $H_2SO_4$ + 1.0 M $CH_3OH$ aqueous solution. (a) Pt–ATO/C, (b) Pt–$SnO_2$/C, and (c) Pt/C.

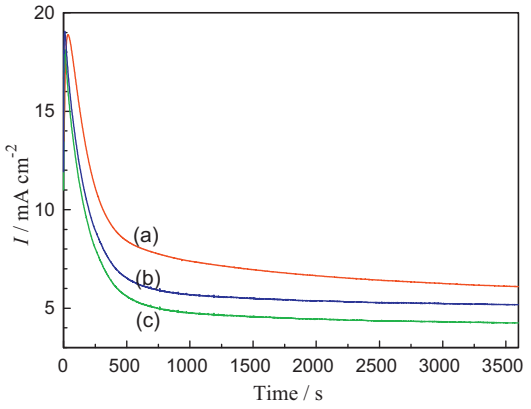


**Fig. 6.** Chronoamperograms of various electrodes at 0.45 V in 1.0 M $H_2SO_4$ + 1.0 M $CH_3OH$ aqueous solution. (a) Pt–ATO/C, (b) Pt–$SnO_2$/C, and (c) Pt/C.

composites show much higher activity than either Pt–$SnO_2$/C or Pt/C.

Fig. 6 shows the current-decay pattern for the three catalysts. Apparently, the current first rapidly attenuates within 10 min, and then the attenuation slows due to catalyst poisoning by the chemisorbed carbonaceous species and the depletion of the OH sites that are responsible for oxidation of CO. Pt–ATO/C has the highest current density among the three catalysts. The catalytic activity of Pt–ATO/C is much higher than that of Pt–$SnO_2$/C and Pt/C due to the enhanced bifunctional mechanism and the relatively high conductivity of ATO/C composites, which is consistent with the CV results.

## 4. Conclusions

In summary, an ATO/C-supported Pt catalyst was conveniently synthesized by co-precipitation. Pt was dispersed on the ATO/C composite surface with a diameter of 8.6 nm. The Pt–ATO/C composites exhibit a relatively high methanol electro-oxidation activity compared to Pt–$SnO_2$/C or commercial Pt/C. The application of antimony-doped metal oxides, such as ATO as co-catalyst of Pt, is a promising and a convenient methanol-oxidation anode catalyst. These efforts aid the development of the present catalyst system and the understanding of surface-site interactions.

## Acknowledgments

Financial support of this work is provided by NSFC (50873021), Shuguang Plan (09SG30), Program for New Century Excellent Talents in University (NCET-06-0421), Shanghai Leading Academic Discipline Project (B603) and the 111 Project (111-2-04).

## References

[1] S. Wasmus, A. Küver, J. Electroanal. Chem. 461 (1999) 14–31.
[2] A. Heinzel, V.M. Barragán, J. Power Sources 84 (1999) 70–74.
[3] L. Liu, C. Pu, R. Viswanathan, Q.B. Fan, R.X. Liu, E.S. Smotkin, Electrochim. Acta 43 (1998) 3657–3663.
[4] E. Antolini, Mater. Chem. Phys. 78 (2003) 563–573.
[5] K.M. McGrath, G.K.S. Prakash, G.A. Olah, J. Ind. Eng. Chem. 10 (2004) 1063–1080.
[6] Z.L. Liu, B. Guo, L. Hong, T.H. Lim, Electrochem. Commun. 8 (2006) 83–90.
[7] C. Bock, C. Paquet, M. Couillard, G.A. Botton, B.R. MacDougall, J. Am. Chem. Soc. 126 (2004) 8028–8037.
[8] Z.Y. Wang, G. Chen, D.G. Xia, L.J. Zhang, J. Alloys Compd. 450 (2008) 148–151.
[9] H.J. Kim, D.Y. Kim, H. Han, Y.J. Shul, J. Power Sources 159 (2006) 484–490.
[10] C.S. Chen, F.M. Pan, Appl. Catal. B: Environ. 91 (2009) 663–669.
[11] T. Maiyalagan, K.F. Nawaz, Catal. Commun. 10 (2009) 433–436.
[12] P. Justin, R.G. Ranga, Catal. Today 141 (2009) 138–143.
[13] Y.X. Bai, J.J. Wu, J.Y. Xi, J.S. Wang, W.T. Zhu, L.Q. Chen, X.P. Qiu, D.J. Guo, Electrochem. Commun. 7 (2005) 1087–1090.
[14] Y.X. Bai, J.J. Wu, J.Y. Xi, J.S. Wang, W.T. Zhu, L.Q. Chen, X.P. Qiu, D.J. Guo, Appl. Catal. B: Environ. 89 (2009) 597–601.
[15] M.S. Saha, R.Y. Li, X.L. Sun, Electrochem. Commun. 9 (2007) 2229–2234.
[16] X.Z. Chui, F.M. Cui, Q.J. He, L.M. Guo, M.L. Ruan, J.L. Shi, Fuel 89 (2010) 372–377.
[17] T.J. Liu, Z.G. Jin, L.R. Feng, T. Wang, Appl. Surf. Sci. 254 (2008) 6547–6553.
[18] Y.W. Huang, Q. Zhang, G.F. Li, M. Yang, Mater. Charact. 60 (2009) 415–419.
[19] T. Morteza, S.K. Sadrnezhaad, J. Power Sources 196 (2011) 399–404.
[20] G. Korotcenkov, D.H. Sang, Mater. Chem. Phys. 113 (2009) 756–763.
[21] K.S. Lee, I.S. Park, Y.H. Cho, D.S. Jung, N. Jung, H.Y. Park, Y.E. Sung, J. Catal. 258 (2008) 143–152.
[22] H.L. Pang, X.H. Zhang, X.X. Zhang, B. Liu, X.G. Wei, Y.F. Kuang, J.H. Chen, J. Colloid Interface Sci. 319 (2008) 193–198.
[23] A.F. Shao, Z.B. Wang, Y.Y. Chu, Z.Z. Jiang, G.P. Yin, Y. Liu, Fuel Cells 10 (2010) 472–477.
[24] J. Zhang, L. Gao, Mater. Res. Bull. 39 (2004) 2249–2255.
[25] Y. Wang, T. Chen, Electrochim. Acta 54 (2009) 3510–3515.
[26] T. Krishnakumar, R. Jayaprakash, N. Pinna, A.R. Phani, M. Passacantando, S. Santucci, J. Phys. Chem. Solids 70 (2009) 993–999.